DOI : https://doi.org/10.56452/6-2-17

ISSN: 0974-5823 Vol. 6 No. 2 September 2021

International Journal of Mechanical Engineering

MEASUREMENT AND ANALYSIS OF ELECTRIC SIGNAL TRANSMISSION USING HUMAN BODY AS MEDIUM FOR WBAN APPLICATIONS

[1]Dr.T.S.Akheel,[2]K.Shamshad bhanu,[3]S.FEROZ SHAH AHMED

[1]Professor,[23]Assistant Professor, Department of ECE
Dr. K V Subba Reddy Institute Of Technology

ABSTRACT
By employing the human body as a transmission channel instead of wired or wireless connections, human body communications (HBCs) enable wire-less body area networks (WBANs). Previous research have provided a variety of methods for measuring and analysing the human body channel, but in order to get useful design parameters for a desired communication system, further interpretations of their findings are still needed. In the IEEE standard 802.15.6 for WBAN, the suggested channel measurement for capacitive coupling HBC adopting digital transmission is used to provide detailed design requirements. In the tests, a battery-operated apparatus with a ground-electrode size of 27–50 mm2 was used to transmit personalised channel-sounding signals to the human body. The signals that were received after passing through the body were measured under 30 different measurement settings that were based on the positions of the transmitter and receiver in relation to the body. The transmission signals' operational frequency might vary by up to 100 MHz. In order to attain the highest possible data rate, this study generates the minimum necessary lengths of symbol-codes based on analyses of channel-measured data in terms of measurement circumstances, operating frequencies, and bandwidths of a receive-filter. Depending on the transmitter topologies, this was done to assure handling of inherent signal faults such as those caused by inter-symbol interference and to give more dependable bit-error-rate performance in the human body channel.

Index Terms: Capacitive coupling, channel measurement, channel modelling, digital transmission, wearable device, wireless body area networks, and human body channel.

I. INTRODUCTION

ONE of the main roles of health-care systems is timely detection of abnormal symptoms stemming from med-ical problems in the human body and the provision of decisive information to treat diseases in the early stages for more effective treatment. The sensors embedded in wearable devices share the monitored health-care information with other sensor nodes, and deliver it to supervising devices, such as a smartphone or smartwatch, which collect and ana-lyze the information based on wireless body area net-works (WBANs) [1]–[3]. These provide low-implementation complexity and low-power consumption for communications. Human body communication (HBC) is an enabling tech-nology to implement WBAN, using the

DOI : https://doi.org/10.56452/6-2-17

human body as a transmission medium [4], [5]. To embody a reliable HBC application with the desired performance and stability, channel characteristics should be investigated prior to designing system specifications. The properties of the human body channel are highly dependent on signal transmission conditions such as postures of the human body [6] as well as the locations of the transmitter (Tx) and receiver (Rx) on the body [7]–[9]. In addition, the signal-design parameters such as modulation technique, data rate, bandwidth, and center frequency of the transmission signal should be determined to be suitable for the channel conditions [10]. Hence, the methods used for channel measurement and the analysis to achieve accurate channel modeling have been essential issues for effective HBC implementation.

The channel model for HBC is mainly divided into the signal transmission methods for capacitive coupling and for galvanic coupling [10], [11]. Capacitive coupling trans-mits signals by making a current loop through an external ground [12]–[14], and galvanic coupling considers the human body as a waveguide and creates a signal path by coupling alternating current into the human body [15]. It has been shown that capacitive coupling achieves better performance in the frequency range over 60 kHz for high data rates, compared to galvanic coupling [10], [11]. Hence, in this paper, the focus is on capacitive coupling as a transmission method to cover required data rates up to megabit per second in applications for WBAN [2], [3], [16].

Previous studies have contributed to the development of measurement setups dedicated to the human body channel, and presented their unique channel properties by analyzing measured data. The impulse response models can be applied to analyze the signal loss over a continuous frequency domain, as well as delay parameters such as coherence bandwidth, mean delay, and root-mean-square (rms) delay spread [17]. In [18], the impulse response of the human body was mod-eled based on the empirically measured data of 70 human subjects with the received narrow pulse signal passed through the human body. With statistical analysis of the measured data, the channel model document of the IEEE standards 802.15.6 for WBAN presented equations for the generation of impulse response for HBC in terms of the ground-electrode sizes of the Tx and Rx, and the distances between Tx and Rx [8]. In [7], the path loss for each discrete frequency was measured in relation to the handling of signal electrode and ground electrode, and to the places where the electrodes were attached to the body. The measured results were used to provide physical interpretation of the human body channel, such as equivalent circuit models [12], [14], and to provide the signal propagation mechanism using electric field equa-tions [19]. However, these previous results did not deal with the analysis of practical parameters for a target HBC system, which is necessary to verify the feasibility of implementation.

The digital transmission scheme, invented as a customized approach for the HBC channel, has contributed to lower complexity and reduced power consumption by excluding a digital-to-analog converter, an analog-to-digital converter, and radio frequency (RF)-related blocks [3], [20]–[24]. The earlier approaches used conventional modulation techniques in wireless communications, such as ON–OFF keying [4], [25], frequency-shift keying [26], and phase-shift keying [27]. Frequency-selective (FS) digital transmission (FSDT), a fun-dament scheme used for digital transmissions of HBC, has been adopted as an HBC Tx in the IEEE standards 802.15.6 for WBAN [3]. Based on the FSDT, the recent approaches have presented enhanced Tx structures for increasing data rates [21], [22], reducing the detection complexity defined as the length of the hamming

DOI : https://doi.org/10.56452/6-2-17

distance (HD) computation [23], and improving spectral efficiencies [24].

The goal of the work reported in this paper is to provide accurate values of minimum symbol-code lengths based on the measurements, enabling to achieve the maximum data rate in a given operating frequency fop with robustness against signal distortions by the human body channel and the band-limit effects of a receive filter, for capacitive coupling HBC based on digital transmission. With consideration of the various postures of the human body and the locations of devices on the body, the channel was measured in terms of frequencies of transmission signal with fops up to 100 MHz through a proposed training signal applied by a signal-generating device with a size of 27 × 50 mm2 powered by a lithium-polymer battery with a nominal voltage of 3.7 V. The experiments were conducted in an RF shielding room to avoid interference signals, which is electromagnetic waves generated by various electronic devices around the user [28]–[30], from being added to the received signal for the channel measurement. The proposed signal processing is able to determine the dominant causes of signal errors using the results of analysis of the achievable energy per bit to noise power spectral density (PSD) ratio (Eb/ N0) depending on the measurement conditions, and intersymbol interference (ISI) effects on the received signal. In addition, the bit-error-rate (BER) performance is evaluated to verify communication reliability with respect to the Tx structures.

The rest of this paper is organized as follows. Section II explains the HBC system model along with a brief review of the recent results of the channel measurement using capacitive coupling, and digital transmission schemes. Section III describes the measurement setup with details of the experimental procedure and the design method of the transmis-sion signal for the channel measurement. The analysis results using signal processing of the measured signal are shown in Section IV. Section V presents the performance evaluations after applying the measured channel effects, in terms of the Tx structures. The conclusion is given in Section VI.

II. SYSTEM MODEL OF HBC

The HBC system can be specified by two elements: the sig-nal transmission method as either capacitive coupling or gal-vanic coupling, and the modulation technique used to transmit information in the signal. This paper deals with capacitive coupling, rather than galvanic coupling, because of its better performance at high data rates in the frequency range higher than 60 kHz [10], [11], and the digital signal transmission considering its contribution to lower complexity and power consumption for the implementation of HBC systems [3], [24].

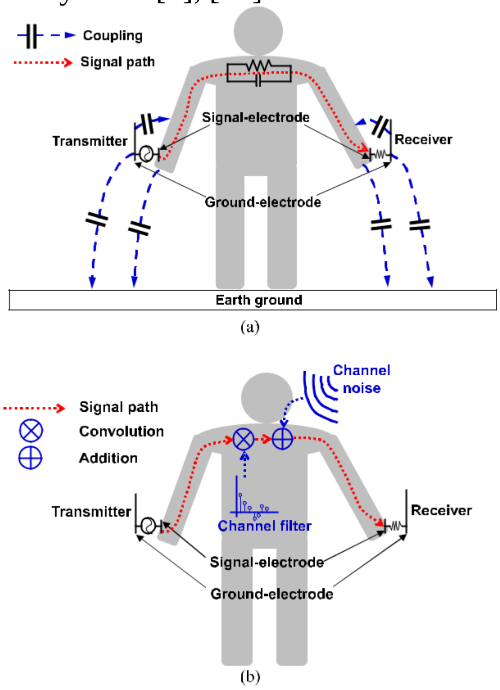

Fig. 1. Channel models for the human body. (a) Electric field formation in capacitive coupling HBC. (b) Channel filter model of HBC.

A. HBC Model of Capacitive Coupling

Fig. 1(a) shows the electric field formation in a capacitive coupling HBC [11], [12]. For both sides of the Tx and Rx, the signal

DOI : https://doi.org/10.56452/6-2-17

electrode is attached to the body to apply and receive an electric signal, while the ground electrodes are floated. The electric signal from the Tx signal electrode creates a

TABLE I:SUMMARY OF CAPACITIVE COUPLING CHANNEL MODELING WORK

Work	Measurement Subject	Measured data and analysis
[8]	Impulse response	Equations for generating impulse response in terms of distance and ground-electrode size of the Tx and Rx
[7]	Path loss	Path loss according to frequency and location of the Tx and Rx on the body
[12]	Path loss and capacitance	Interpretation of the human body channel as circuit models
[19]	Path loss	Verifying theoretical formulations of path loss in terms of the distance between the Tx and Rx, and according to frequency
[17]	Impulse response	Delay properties of the impulse response such as coherence bandwidth, mean delay, and RMS delay spread
[18]	Impulse response	Modeling of the impulse response generated by a series of random variables using measurements of 70 human subjects

difference of electric potential between the human body and the Tx ground electrode coupled with the earth ground. The signal is delivered to the Rx by detecting changes of the electric field produced between the signal electrode and ground electrode of the Rx. The amplitude of the received signal becomes greater as the signal electrode and ground electrode for both sides of the Tx and Rx are closely coupled with the human body and earth ground, respectively. Hence, variations in capacitance caused by different postures of the human body and by environmental variation result in differences of the channel properties.

Fig. 1(b) shows a channel filter model of HBC when the sig-nal is transmitted between the wrists. The HBC channel model using capacitive coupling can be simplified by presenting the signal paths, including through the air and on the body, as a channel filter expressed as a finite impulse response (FIR) [8]. The channel noise, including electromagnetic waves generated from various electronic devices, is absorbed into the body due to the antenna effects of the human body [28]–[30], which can be modeled as an additive white Gaussian noise (AWGN) [8]. While the tap coefficients of the impulse response of the human body channel are not determined linearly, the received signal can be presented as

$$y_k = \sum_{i=0}^{L-1} h_i x_{k-i} + n_k \qquad (1)$$

where y is the output signal, x is the input signal, h is a channel filter represented by an FIR filter of a causal system with L multipath terms, and n is the additive channel noise.

Table I presents previously published work on the HBC channel models. The HBC channel model for WBAN

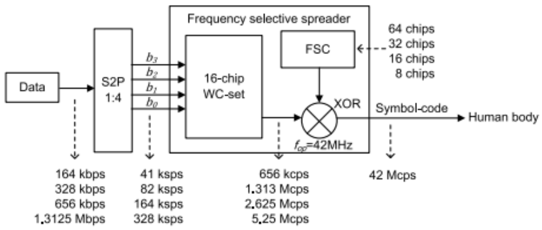

Fig. 2. Tx block diagram of the FSDT for the IEEE standards 802.15.6 for WBAN.

presented equations for the generation of the impulse response in terms of the distance between the Tx and Rx, and the size of the ground electrodes of both sides of the Tx and Rx over the frequency range between 5 and 50 MHz [8]. In [7], the channel path loss was measured in terms of the transmission distance and frequency difference. With results relevant to the path loss, the signal transmission mechanism was analyzed as equivalent circuit models [12] and electric field equations [19]. The impulse response models can give time-delay properties such as mean delay, rms delay spread, and analysis on the coherence bandwidth [17]. The empirical channel model based on the impulse response model was presented with respect to data from multiple subjects of 70 humans in [18]. While these measured data give meaningful physical properties of the HBC channels, more

DOI : https://doi.org/10.56452/6-2-17

interpretation work, accompanied by suitable signal processing is required to obtain reference values for design parameters, and to use them to evaluate system performance.

B. Digital Transmission Schemes

Fig. 2 shows a Tx block diagram of the FSDT in the IEEE standards 802.15.6 for WBAN [3], as one of basic structures of digital transmission. The baseband data enter a serial-to-parallel block to form a 4-bit parallel signal. The 4 bit is mapped to a 16-bit Walsh code (WC), and then spread by frequency-shift code (FSC) of a [0 1] repeated code. For example, the eight-chip FSC code is [0 1 0 1 0 1 0 1], where the chip means a pulse of a rectangular digital signal in the spreading process. The data rate is varied by the length of the FSC. The spread code is defined as a symbol code. Table II presents a comparison of variations of digital transmission schemes based on capacitive coupling. In [20], the Tx structure was simplified by mapping information bits to a 64-chip WC without a spreading process, but the data rate was fixed. The parallelized multispreader increased a maximum data rate up to 3 times higher than that of the FSDT with the three FS spreaders arranged in parallel [21]. The multilevel baseband coding increased the data rate by combining two WCs into a three-level signal [22]. The structure for reducing the detection complexity of the length of the HD computation was pre-sented in [23]. The narrowband digital transmission (NBDT) improved the spectral efficiency by direct spreading of infor-mation bits using the FSC without WC [24]. One of the common features of the digital transmission schemes for HBC is that if the center frequency determined by half fop is

TABLE II COMPARISON OF DIGITAL TRANSMISSION SCHEME

Work	Transmission scheme	f_{op} (MHz)	Maximum data rate (MBPS)	3 dB bandwidth (MHz)
[3]	FSDT	42	1.3125	18.375 − 23.625
[20]	Using fixed chip length WC	32	2	8 − 22
[21]	Multi-spreader	42	3.9375	15.75 − 26.25
[22]	Multi-level baseband coding	160	60	n.a.
[23]	Using half number of WC	42	1.3125	18.375 − 23.625
[24]	Narrow band transmission	42	1.3125	20.34375 −21.65625

n.a. = data not available.

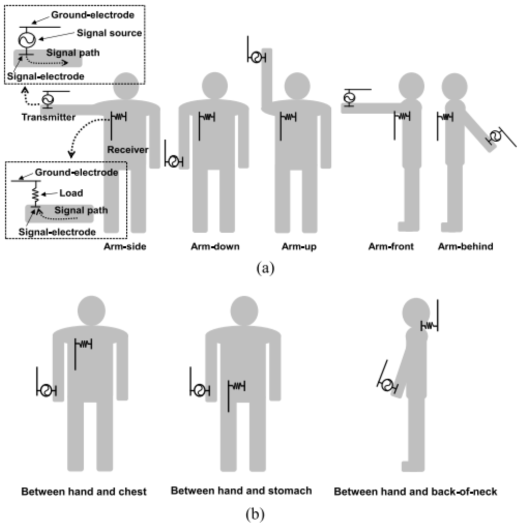

Fig. 3. (a) Postures for the channel measurement of the human body.(b) Device locations for the channel measurement of the human body.

fixed, the data rate increases linearly with decrease in the length of the symbol code. Hence, an accurate estimation of the minimum length of the symbol code satisfying a desired detection performance is a significant factor for achieving the maximum available data rate in a given fop.

III. MEASUREMENT METHOD

A. Setup for Channel Measurement

Properties of the human body channel are easy to vary with the body postures and locations of the devices on the body,

DOI : https://doi.org/10.56452/6-2-17

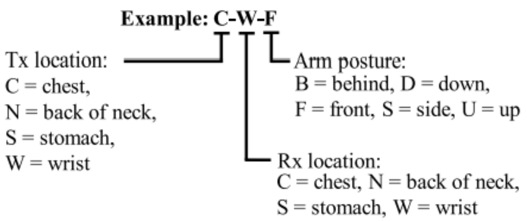

Fig. 4. Simplified expression for a measurement condition.

leading to changes in the distance between the Tx and Rx, and capacitance between ground electrodes of both sides of the Tx and Rx and the earth ground. Hence, the experiments included five arm postures including arm side, arm down, arm up, arm front, and arm behind as shown in Fig. 3(a), where the Tx and Rx were placed on the hand and chest, respectively, as an example. This paper assumes that the device on the hand, such as a smartphone or smartwatch, creates communication channels with the devices on the body as shown in Fig. 3(b), where the roles of the Tx and Rx are exchangeable. The other device was placed at one of three locations on the upper part of the body including the chest, stomach, and back of the neck considered poor channel conditions, where the channel attenuation decreases as the ground electrode of the device moves closer to the earth ground [7]. In capacitive coupling, the human body channel is known to be affected independently by the size of each ground electrode of the Tx and Rx [8]. The intrinsic capacitance placed inside the body in Fig. 1(a), modeled basically by the electrical properties of the tissues, can be considered static. This means that the intrinsic capacitance is not affected by external conditions, being only dependent on the distance of propagation over the body [12]. The channel differences depending on the trans-mission directions are dominated by the extrinsic capacitance induced by different external relations of the electric coupling between the earth ground and the ground electrode of each Tx and Rx, rather than the intrinsic capacitance of the human body. For example, for the channel path over the arm parallel to the earth ground, there is no reason that the channel should be asymmetric assuming the same external capacitance for the Tx and Rx based on a relatively short channel distance and the same external environmental conditions for the Tx and Rx, such as height between the earth ground and the body. This study considers the channel paths between the chest and the wrist, the stomach and the wrist, and the back of neck and the wrist, with various postures. Since there are observable external environmental differences between the earth ground and the ground electrode of each Tx and Rx leading to differences of external capacitance between the Tx and Rx, the channel properties are expected to be different depending on the measurement direction. Hence, the human body channel is evaluated in terms of the transmission direction with the overall number of measurement cases of 30. Fig. 4 shows a simplified expression for the measurement condition. For example, C-W-F means that a signal transmits from the Tx on the chest to the Rx on the wrist in the arm-front posture. The device location of the wrist is assumed to be effectively the same as that of the hand.

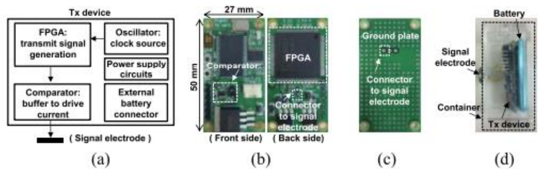

Fig. 5. (a) Block diagram of the Tx device for the channel measurement.(b) Tx device for the channel measurement. (c) Rx device for the channel measurement. (d) Tx device in the transparent container.

DOI : https://doi.org/10.56452/6-2-17

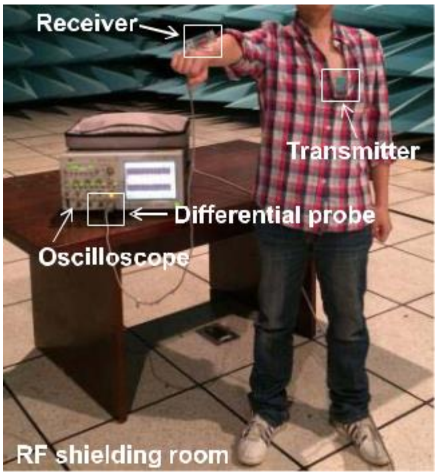

Fig. 6. Measurement setup of the channel measurement of C-W-F in the RF shielding room.

Fig. 5(a)–(c) shows the Tx block diagram, Tx device, and Rx device for the channel measurement, respectively. In the Tx, transmission signals were generated using an FPGA of XC3S200 [31], and a comparator of TLV3501 [32] was employed as an output buffer to enhance the current driving capacity when the Tx signal was applied to the body. The size of the ground electrode, equivalent to that of the device, was 27 × 50 mm2. The Rx was composed of the signal electrode, and ground electrode of the same size as those of the Tx. The signal electrodes of the Tx and Rx were attached to the body using one-point electrocardiogram monitoring electrodes. The devices were put in a transparent nonconducting container, as shown in Fig. 5(d), to lower electric coupling between the ground electrode and the human body surface by secur-ing distance between them. The container included a 3.7-V lithium-polymer battery. Fig. 6 shows an experimental setup of the channel measurements, when the measurement condition was C-W-F. The experiment was conducted in an RF shielding room, to maintain high signal-to-noise ratio (SNR) at the Rx by minimizing the channel noise. The room size was large enough to be unaffected by the effects of signal enhancement by nearby walls, which cause an artificial increase of the electric coupling between the ground electrode of the device and earth ground, leading to the improved amplitude of the received signal. When the signal was measured, the signal electrode of the Rx was connected to an oscilloscope using a differential probe to isolate the ground electrode between the Rx and measurement equipment [17], [18], [30].

B. Design of Transmission Signal for Channel Measurement

In the digital transmissions for HBC, the maximum number of consecutive 0s and 1s is limited to two in the transmission

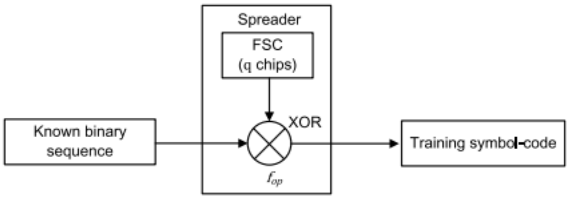

Fig. 7. Block diagram of the TSC generator.

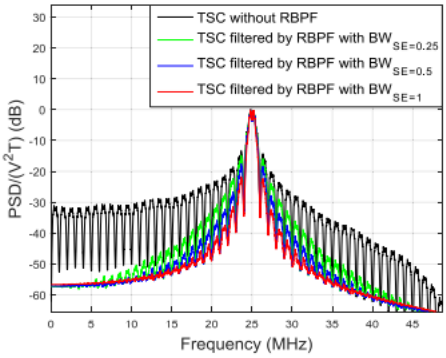

Fig. 8. Power spectrums of the TSC, TSC filtered by RBPF with BWSE=0.25, TSC filtered by RBPF with BWSE=0.5, and TSC filtered by RBPF with BWSE =1.

signal to minimize bandwidth, and to lessen ISI effects on the received signal, where the ISI is induced by FS fading characteristic of the human body channel [17], and band-limit effect by a receive filter [24]. The receive filter is required to stabilize the fluctuation of the ground signal level, and to improve SNR at the Rx by rejecting the channel noise outside the

DOI : https://doi.org/10.56452/6-2-17

frequency band of the desired signals. While the repeated binary pattern (RBP) of [0 0] and [1 1] causes burst chip errors due to ISI in the symbol code, the transmission signal must contain RBPs to deliver information data, where the RBP occurs when the input bit is inverted from 0 to 1, or 1 to 0, and the number of RBPs increases as the data rate increases.

Fig. 7 shows a block diagram for generating a training symbol code (TSC) adopting the conventional Tx structure of the NBDT [24]. The minimum required length of a symbol code can be estimated by counting the chip errors in the received TSC passed through the human body. Each bit from the known binary sequence is spread by the FSC with a spreading factor q, and the spread code is defined as a TSC. The fundamental frequency of the TSC is determined by a half frequency of fop. The known binary sequence keeps changing between 0 and 1 to generate consecutive RBPs in every symbol boundary, to set the condition of the most error-prone input pattern. The bandwidth BWSE =α , satisfied with the spectral efficiency α based on 3-dB bandwidth centered on the frequency of fop/2, is presented as

$$\mathrm{BW}_{\mathrm{SE}=\alpha} = \frac{1}{\alpha} \times \frac{1}{q} \times f_{\mathrm{op}}. \qquad (2)$$

The experiments were conducted in terms of fop up to 100 MHz, and receive-band-pass filters (RBPFs) with BWSE=1, BWSE=0.5, and BWSE=0.25, designed as a Butterworth infinite impulse response (BIIR)-type filter, to investigate the effects of the RBPFs on the received TSC with BWSE=1 of 1 MHz. Fig. 8 shows PSDs of a received TSC signal filtered by the RBPFs with BWSE=1, BWSE=0.5, and BWSE=0.25, where T is the sampling rate and V is the binary 1-V level. The center frequency and data rate of the TSC are 25 MHz and 1 Mb/s, respectively, and the RBPF uses a BIIR-type filter with the filter order of 2. While securing a higher spectral efficiency, the narrower bandwidth of the RBPF removes more of the desired signals and incurs greater signal distortions, leading to performance degradation. The TSC was transmitted on a frame-by-frame basis, where one frame was composed of 64 TSCs, followed by a null period, composed of 512 chips of zeros.

IV. MEASUREMENT AND ANALYSIS

A. Signal Processing of Measured Data

In an HBC system powered by a battery, the ground electrodes of both devices of the Tx and Rx are floated, and the received signal swings around the floating voltage of the ground electrode of the Rx. For example, Fig. 9(a) shows a measured received TSC signal from the experiment of C-W-F, where fop is 50 MHz and the sampling rate of the measurement instrument fsi is 2 GHz. An RBPF filters the received signal to detect voltage differences between the signals received from the Tx and the ground electrode of the Rx. Fig. 9(b) shows the signal in Fig. 9(a), filtered by applying the RBPF designed as a BIIR-type filter, where the filter order is 2, fsi is 2 GHz, and BWSE=1 is 1 MHz with lower cutoff frequency of 24.5 MHz and upper cutoff frequency of 25.5 MHz. Excessively high fsi compared to fop causes processing complexity to increase due to redundant samples. Fig. 9(c) shows a decimation process, where the sampling rate is reduced from 2 GHz to 50 MHz. By aid of signal processing, the signal received can be recognized as a binary signal of 0 or 1 by detecting the value of every peak-to-peak voltage. In the case that the decimation ratio fsi/ fop is not divided by an integer value, the decimation process should include an operation of periodic compensation for the delayed or preceded sampled signal due to sampling offsets. The decimated signal is determined to be a binary signal by the reference voltage of 0 V as shown in Fig. 9(d), where there is no hysteresis in the comparator due to a high-SNR condition, and filtering delays are compensated for explicit check of the

DOI : https://doi.org/10.56452/6-2-17

number of chip errors. The number of chip errors incurred by an RBP can be counted by comparing the binary decision signal with the known transmitted TSC signal from the Tx. Frame synchronization is achieved by detecting the chip location, which records a maximum correlation value between the known binary sequence and the received decimation signal in Fig. 9(c).

Fig. 9. (a) Measured received signal of the experiment C-W-F. (b) Band-pass filtering process. (c) Decimation process. (d) Comparison between the transmitted binary signal and binary decision signal on the decimation signal after compensation of filtering delays

B. Measurement of Eb/ N0

Fig. 10(a) and (b) shows average Eb/ N0 over fop versus the index of the measurement condition presented in Table III, and average Eb/ N0 over the index of the measurement con-dition versus fop, respectively, in terms of bandwidths of the RBPF. As shown in Fig. 4, the first, second, and third alphabets of the index of the measurement condition indicate the Tx location, Rx location, and arm posture, respectively.

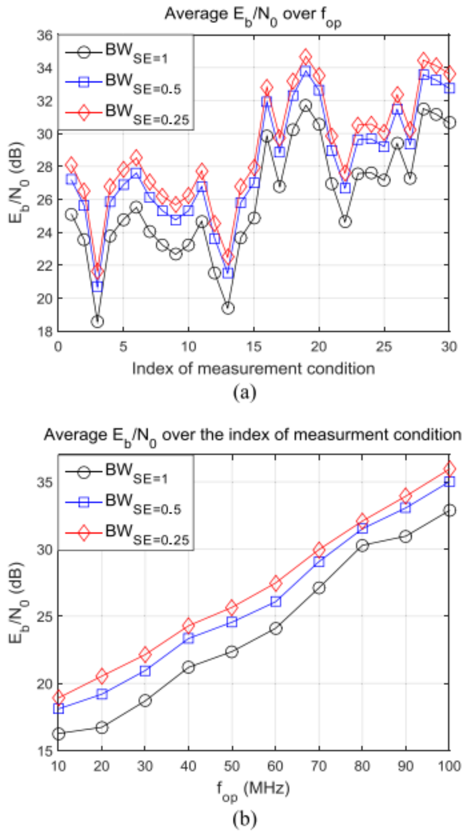

Fig. 10. (a) Average Eb / N0 s over fop versus the index of the measurement condition. (b) Average Eb / N0s over the index of the measurement condition versus fop.

The Tx and Rx locations include the chest (C), back of neck (N), stomach (S), and wrist (W), and the arm posture considers behind (B), down (D), front (F), side (S), and up (U). The average Eb/ N0 is the mean value of Eb/ N0 for the period of 640 TSCs applying RBPFs with BWSE=1, BWSE=0 .5, and

TABLE III INDEX OF MEASUREMENT CONDITION

Index	Condition	Index	Condition	Index	Condition
1	C-W-B	11	S-W-B	21	W-N-B
2	C-W-D	12	S-W-D	22	W-N-D
3	C-W-F	13	S-W-F	23	W-N-F
4	C-W-S	14	S-W-S	24	W-N-S
5	C-W-U	15	S-W-U	25	W-N-U
6	N-W-B	16	W-C-B	26	W-S-B
7	N-W-D	17	W-C-D	27	W-S-D
8	N-W-F	18	W-C-F	28	W-S-F
9	N-W-S	19	W-C-S	29	W-S-S
10	N-W-U	20	W-C-U	30	W-S-U

DOI : https://doi.org/10.56452/6-2-17

BWSE=0.25 centered on the fop/2 MHz. The average signal power of the channel noise Pnoise is calculated using the measured received signal in the period where the TSCs are not contained between frames. In addition, the average TSC signal power PTSC is computed from the measured received TSCs contained in frames. PTSC/ Pnoise, equivalent to carrier-to-noise ratio (CNR), is related to the Eb/ N0 as follows:

$$\mathrm{CNR} = \frac{E_b}{N_0} \cdot \frac{f_b}{B} \tag{3}$$

$$\frac{E_b}{N_0} = \mathrm{CNR} \cdot \frac{B}{f_b} = \frac{P_{\mathrm{TSC}}}{P_{\mathrm{noise}}} \cdot \frac{B}{f_b} \tag{4}$$

where fb is the bit rate of the TSC and B is the channel bandwidth [33]. The Eb/ N0 values higher than 16 dB confirm the assumption that the experiments in the RF shielding room maintain high Eb/ N0 conditions. Hence, chip errors are mainly caused by the effects from the human body channel and RBPF, rather than by the channel noise under these E b/ N0 conditions [24], [30]. Fig. 10(a) shows that the path loss is dependent on the transmission directions even for the same locations of the Tx and Rx. The signal transmissions from the wrist to a place on the torso, indexes between 16 and 30, tend to achieve higher Eb/ N0s than those of opposite directions, indexes between 1 and 15. For example, the signal transmissions from the torso to wrist such as C-W-F and S-W-F, indexes 3 and 13, respectively, record low Eb/ N0s, while those of the opposite direction such as W-C-S, index 19, and W-S-F, index 28, achieve high Eb/ N0s. As shown in Fig. 10(b), the Eb/ N0 increases with increased fop, consistent with the characteristics of capacitive coupling, where the path loss of a signal is reduced as the frequency of the signal gets higher [7]. Compared to the average Eb/ N0 of BWSE=1, the average Eb/ N0s of BWSE=0.5 and BWSE=0.25 increase about 2.05 and 3.01 dB, respectively.

C. Measurement of Chip Error

To ensure correct symbol-code detection in the Rx for all of the 30 measurement conditions, and for variations of fop, the symbol code should be designed to overcome the worst situation considering the maximum possible number of chip errors, rather than average chip errors. Even under the same measurement condition, the measured data cannot show the same results due to randomly determined experimental factors, such as unintended movement or trembling of the body, which cause changes to the signal paths in the body channel and electric coupling conditions between ground electrodes of devices and the earth ground. Hence, the mean values of the number of measured chip errors can be assumed to follow Gaussian distributions according to the central limit theorem. The maximum possible number of chip errors in one TSC is defined as the maximum value in the 99% confidence interval of chip errors MVCI=99% for mean values of 640 TSCs [34].

Fig. 11 shows MVCI=99% of chip errors in terms of fop and the experimental conditions, using RBPFs with BWSE=1, BWSE=0.5, and BWSE=0.25 centered on fop/2 MHz. The num-ber of chip errors is reduced as the bandwidth of the RBPF widens from BWSE=1 to BWSE=0.25, which lessens the ISI effects triggered by RBPs in the every TSC boundary, as shown in Fig. 9. The distributions of MVCI=99% of chip errors are varied with fop. For fop between 10 and 50 MHz, the indexes from 6 to 10, where the signal is transmitted from the back of neck to the wrist, tend to have higher MVCI =99% of chip errors compared to those of other indexes. C-W-F, index 3, and S-W-F, index 13, record high numbers of chip errors for fop higher than 30 and 60 MHz, respectively. A new peak of MVCI=99% of chip errors occurs at W-N-D, index 22, for fop higher than 80 MHz. The number of chip errors in lower fops including 10 and 20 MHz are smaller than that of

DOI : https://doi.org/10.56452/6-2-17

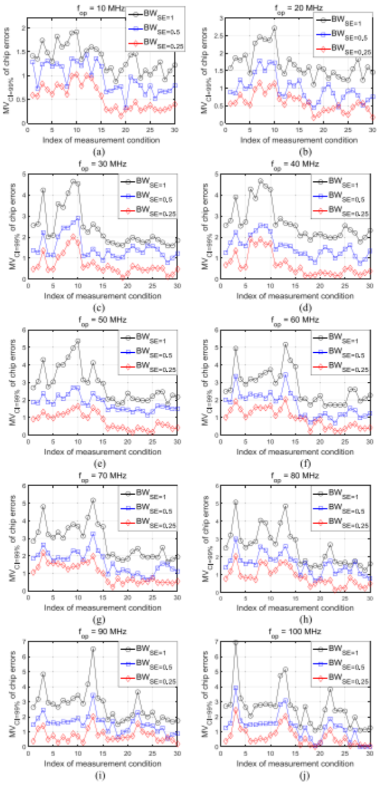

Fig. 11. MVCI=99% of chip errors based on the measurement in terms of fop and the measurement condition. (a) fop = 10 MHz. (b) fop = 20 MHz. (c) fop = 30 MHz. (d) fop = 40 MHz. (e) fop = 50 MHz. (f) fop = 60 MHz. (g) fop = 70 MHz. (h) fop = 80 MHz. (i) fop = 90 MHz. (j) fop = 100 MHz.

higher fops, in accordance with the existing result that the ISI effects become weak as fop lowers [35].

D. Minimum Required Symbol-Code Length

The chip length of the symbol code Lsc with a minimum HD Dmin can be written as

$$L_{sc} = w \times D_{min} \qquad (5)$$

TABLE IV PROPOSED Lsc AND CORRESPONDING Rmax (for Nsc = 2)

f_{op} (MHz)	Minimum required L_{sc} (L_{minsc})			R_{max} (Mbps)		
	$BW_{SE=1}$	$BW_{SE=0.5}$	$BW_{SE=0.25}$	$BW_{SE=1}$	$BW_{SE=0.5}$	$BW_{SE=0.25}$
10	3	3	3	3.33	3.33	3.33
20	5	3	3	4	6.67	6.67
30	9	5	3	3.33	6	10
40	9	5	3	4.44	8	13.33
50	11	5	3	4.55	10	16.67
60	11	7	5	5.46	8.57	12
70	11	7	5	6.36	10	14
80	11	7	5	7.27	11.43	16
90	13	7	5	6.92	12.86	18
100	13	7	5	7.69	14.29	20

where w is an integer value for the factor of a linear increment. If the number of elements in a symbol-code set Nsc is more than two such as the FSDT with Nsc of 16 in [3], the minimum w should be greater than one to satisfy the orthogonality among symbol codes. In the case that Nsc is two, the minimum Lsc is equal to Dmin. For example, the two symbol codes of the NBDT are composed of FSC and bit-inversed FSC [24], identical with the generation method of the TSC in Fig. 7. For perfect detection of the symbol code in the Rx, Dmin should be satisfied in

$$D_{min} = 2e_{max} + 1 \qquad (6)$$

where emax is the maximum number of chip errors, and which can be rearranged using (5) as

$$L_{sc} = w \times (2e_{max} + 1). \qquad (7)$$

With a minimum value of Lsc from (7), the maximum data rate Rmax in terms of fop can be presented as

$$R_{max} = \frac{f_{op}}{L_{sc}} \times \log_2 N_{sc}. \qquad (8)$$

Table IV lists the minimum required Lsc (Lminsc) at each fop to cope with the chip errors induced by the effects of the human body channel and RBPF for the overall indexes of measurement condition based on MVCI=99% of chip errors in Fig. 11, and corresponding Rmax for each fop, in terms of the bandwidths of BWSE=1, BWSE=0.5, and BWSE=0 .25 of the RBPF, when Nsc is 2. While higher fop leads to an improved data rate, it also

DOI : https://doi.org/10.56452/6-2-17

increases the device power consumption by a factor of fop [36]. Moreover, in the case that Nsc is greater than two such as the FSDT [3] with a fixed Nsc of 16, Lminsc offers a reference for the minimum required length of the FSC in Fig. 2 to avoid symbol-code errors resulting in information bit errors.

V. PERFORMANCE EVALUATION BASED ON MEASUREMENT

The evaluation of BER performance is an essential to determine the Tx structure for generating transmission signals satisfying required specifications such as frequency band,

signal bandwidth, and desired BER performance. In digital transmission for HBC, the achievable BER performance for given received signal power can be enhanced by spread-ing gains using more transmission power. While improving detection performance, the greater number of the orthogonal code bits than that of information bits costs a reduction in the data rate. The criterion on the relationship between the amount of SNR gain and loss of data rate is required to obtain a suitable SNR gain for achieving the desired BER in terms of Tx structures, when the Eb/ N0 required for a target BER cannot be secured in the Rx. Hence, this section presents an evaluation of the effects of the human body channel and RBPF on the performance of the two representative digital transmission schemes of the NBDT [24] and FSDT [3], based on analysis of the measurement results.

The received signal can be determined to be a binary signal by employing a comparator and clock-and-data-recovery in the analog front end (AFE) of the Rx [20], [37], [38]. Assuming perfect frame synchronization, a maximum-likelihood detector computes the HD between the hard-decision bit stream from the AFE and all of the candidate symbol-code vectors, and then finds the candidate code vector cˆ satisfying

$$\hat{\mathbf{c}} = \arg\min_{c \in S} d(\mathbf{c}, \mathbf{z}) \qquad (9)$$

where S denotes the set of candidates of symbol-code vectors, d() is the HD between two vectors, and z is the code vector of the hard-decision received signal. The HD computation can be carried out using XOR operation and counting the number of 1s of the two code vectors.

Fig. 12(a) shows comparisons of BER performances versus

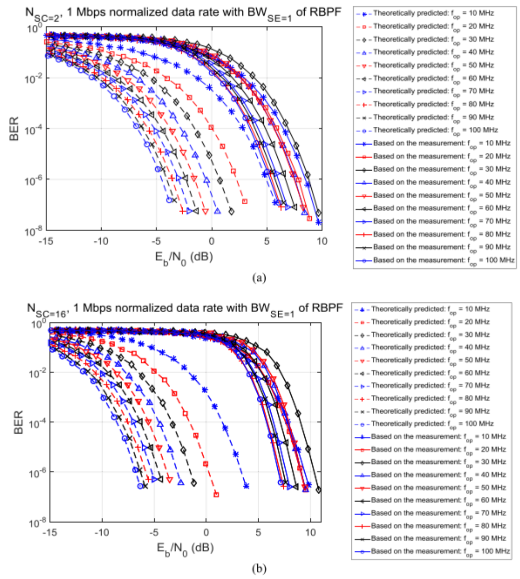

Fig. 12. BER curves based on the measurement versus Eb/ N0 and theoretically predicted BER curves versus Eb/ N0 , with BWSE=1 of the RBPF, in terms of fop. (a) Nsc = 2 for the case of the NBDT Tx with the lengths of the symbol code of L minsc. (b) Nsc = 16 for the case of the FSDT Tx with the lengths of the symbol code of Lminsc × 16.

E b/ N0 in terms of fop with the corresponding Lminsc in Table IV as a symbol-code length, between the BER curves based on the measurement and theoretically predicted BER curves, when Nsc is two and the Tx structure is the NBDT [24]. Since the goal of this paper is to offer reliable values of minimum symbol-code lengths to achieve the maximum data rates ensuring the desired performance, possible worst cases of error

occurrence are considered for the BER curves based on the measurement. Hence, the maximum possible chip errors in Fig. 11 according to fop are applied as the chip errors by the ISI effects from the channel and RBPF. For example,
when fop is 50 MHz with the RBPF of BWSE=1, Lminsc is 11 in Table IV. Without consideration of the effects of the channel and RBPF, the overall length of 11 chips can be used to increase a code distance for spreading gains. However, based on the analysis of the measured data, in the worst condition, only one chip can be available to detect the correct symbol code in the Rx, due to five chip errors by the channel and RBPF as shown in Fig. 11(e). The environment of human body channel noise is equivalent to an AWGN channel [8]. The bandwidth of BWSE=1 of RBPF is the minimum bandwidth required to accommodate the data rate. In the same manner, Fig. 12(b) deals with the results in the case that Nsc is 16 for the Tx structure of the FSDT [3]. Lminsc is adopted as the chip length of the FSC for each fop. Hence, the lengths of the symbol code for the FSDT is 16 × Lminsc. The BER performances in Fig. 12 are calibrated to a normalized data rate of 1 Mb/s over variations of fop, and the noise power is calculated using the noise value passed through the corresponding RBPF.
Neglecting the ISI effects from the channel and filters, the BER performances of the theoretically predicted BER curves in an AWGN channel appear better than the actual results. Hence, the results in this paper can offer more practical BER performance, based on the analysis of the measured data, to achieve a desired performance in real implementations. Compared to the theoretically predicted BER curves, the BER curves based on the measurement degrade the average Eb/ N0 at a BER of 10−6 by about 8.11 dB for the NBDT and 11.77 dB for the FSDT due to the ISI effects form the channel and RBPF as shown in Fig. 12(a) and (b), respectively. Compared to the BER curves based on the measurement of the NBDT in Fig. 12(a), those of the FSDT in Fig. 12(b) degrade the average Eb/ N0 by about 1.50 dB at a BER of 10−6. The BER performances of the FSDT are more affected by the ISI than those of the NBDT, where the bandwidth of the FSDT is 4 times wider than that of the NBDT as presented in Table II.

VI. CONCLUSION

Based on the results of testing under channel changes, this work offered a design guideline of transmission symbol code aimed to obtain a maximum data throughput while ensuring stable operation for capacitive coupling HBC employing digital transmission. Taking into account the change in signal frequencies according to fop from 10 to 100 MHz, the measurements were carried out for 30 different types of measurement circumstances specified by the locations of the Tx and Rx, directions of signal transmission, and postures of the human body. The analysis findings of the Eb/ N0 and MVCI=99% of chip errors with the suggested signal processing on the measured data demonstrate, respectively, the distribution features of the signal route loss and the minimum necessary length of symbol codes needed to prevent symbol mistakes caused by ISI by the RBPs. More realistic BER performance was assessed with account of the Tx structures using analysis based on measured findings.

REFERENCES

[1] C. Otto, A. Milenkovi´c, C. Sanders, and E. Jovanov, “System architecture of a wireless body area sensor network for ubiquitous health monitoring,” J. Mobile Multimedia, vol. 1, no. 4, pp. 307–326, Jan. 2005.
[2] S. Movassaghi, M. Abolhasan, J. Lipman, D. Smith, and A. Jamalipour, “Wireless body area networks: A survey,” IEEE Commun. Surveys Tuts., vol. 16, no. 3, pp. 1658–1686, 3rd Quart., 2014.

[3] IEEE Standard for Local and Metropolitan Area Networks—Part 15.6: Wireless Body Area Networks, IEEE Standard 802.15, Working Group for WPAN, 2012.
[4] T. G. Zimmerman, "Personal area networks: Near-field intrabody com-munication," IBM Syst. J., vol. 35, nos. 3–4, pp. 609–617, 1996.
[5] T. G. Zimmerman, J. R. Smith, J. A. Paradiso, D. Allport, and N. Gershenfeld, "Applying electric field sensing to human-computer interfaces," in Proc. CHI, 1995, pp. 280–287.
[6] Q. Wang, T. Tayamachi, I. Kimura, and J. Wang, "An on-body channel model for UWB body area communications for various postures," IEEE Trans. Antennas Propag., vol. 57, no. 4, pp. 991–998, Apr. 2009.
[7] M. A. Callejon, D. Naranjo-Hernandez, J. Reina-Tosina, and L. M. Roa, "A comprehensive study into intrabody communication measurements," IEEE Trans. Instrum. Meas., vol. 62, no. 9, pp. 2446–2455, Sep. 2013.
[8] Channel Model for Body Area Network (BAN), IEEE Standard P802.15-08-0780-12-0006, Nov. 2010.
[9] M. S. Wegmueller et al., "An attempt to model the human body as a communication channel," IEEE Trans. Biomed. Eng., vol. 54, no. 10, pp. 1851–1857, Oct. 2007.
[10] M. Seyedi, B. Kibret, D. T. H. Lai, and M. Faulkner, "A survey on intrabody communications for body area network applications," IEEE Trans. Biomed. Eng., vol. 60, no. 8, pp. 2067–2079, Aug. 2013.
[11] M. Amparo Callejon, D. Naranjo-Hernandez, J. Reina-Tosina, and L. M. Roa, "Distributed circuit modeling of galvanic and capacitive coupling for intrabody communication," IEEE Trans. Biomed. Eng., vol. 59, no. 11, pp. 3263–3269, Nov. 2012.
[12] M. D. Pereira, G. A. Alvarez-Botero, and F. R. de Sousa, "Characteriza-tion and modeling of the capacitive HBC channel," IEEE Trans. Instrum. Meas., vol. 64, no. 10, pp. 2626–2635, Oct. 2015.
[13] Ž. Luˇcev, I. Krois, and M. Cifrek, "A capacitive intrabody communica-tion channel from 100 kHz to 100 MHz," IEEE Trans. Instrum. Meas., vol. 61, no. 12, pp. 3280–3289, Dec. 2012.
[14] H. Wang, X. Tang, C. S. Choy, and G. E. Sobelman, "Cascaded network body channel model for intrabody communication," IEEE J. Biomed. Health Inform., vol. 20, no. 4, pp. 1044–1052, Jul. 2016.
[15] M. A. Callejón, J. Reina-Tosina, D. Naranjo-Hernández, and L. M. Roa, "Measurement issues in galvanic intrabody communication: Influence of experimental setup," IEEE Trans. Biomed. Eng., vol. 62, no. 11, pp. 2724–2732, Nov. 2015.
[16] H. Baldus, S. Corroy, A. Fazzi, K. Klabunde, and T. Schenk, "Human-centric connectivity enabled by body-coupled communications," IEEE Commun. Mag., vol. 47, no. 6, pp. 172–178, Jun. 2009.
[17] J.-H. Hwang, T.-W. Kang, Y.-T. Kim, and S.-O. Park, "Measurement of transmission properties of HBC channel and its impulse response model," IEEE Trans. Instrum. Meas, vol. 65, no. 1, pp. 177–188, Jan. 2016.
[18] J. H. Hwang, T. W. Kang, S. O. Park, and Y. T. Kim, "Empirical chan-nel model for human body communication," IEEE Antennas Wireless Propag. Lett., vol. 14, pp. 694–697, 2015.
[19] J. Bae, H. Cho, K. Song, H. Lee, and H.-J. Yoo, "The signal trans-mission mechanism on the surface of human body for body channel communication," IEEE Trans.

DOI : https://doi.org/10.56452/6-2-17

Microw. Theory Techn., vol. 60, no. 3, pp. 582–593, Mar. 2012.
[20] C.-H. Hyoung, S.-W. Kang, S.-O. Park, and Y.-T. Kim, "Transceiver for human body communication using frequency selective digital transmis-sion," ETRI J., vol. 34, no. 2, pp. 216–225, Apr. 2012.
[21] T. Kang, I. Lim, J. Hwang, C. Hyoung, H. Park, and S. Kang, "A method of increasing data rate for human body communication system for body area network applications," in Proc. IEEE Veh. Technol. Conf., Sep. 2012, pp. 1–5.
[22] C. K. Ho et al., "High bandwidth efficiency and low power consumption Walsh code implementation methods for body channel communication," IEEE Trans. Microw. Theory Techn., vol. 62, no. 9, pp. 1867–1878, Sep. 2014.
[23] T.-W. Kang et al., "A complexity-efficient human body communi-cations," in Proc. IEEE Asia–Pacific Conf. Commun., Aug. 2013, pp. 445–446.
[24] T.-W. Kang et al., "Highly simplified and bandwidth-efficient human body communications based on IEEE 802.15.6 WBAN standard," ETRI J. , vol. 38, no. 6, pp. 1074–1084, Dec. 2016.
[25] C. H. Hyoung, J. B. Sung, J. H. Hwang, J. K. Kim, D. G. Park, and S. W. Kang, "A novel system for intrabody communication: Touch-and-play," in Proc. IEEE Int. Symp. Circuit Syst., May 2006, pp. 1343–1346.